Heat-Treatment Effect on Phase Stability, Cation Distribution, Chemical Composition, and Electrochemical Behavior for Fe-Substituted Li_2MnO_3

Mitsuharu Tabuchi,* Akiko Nakashima, Kazuaki Ado, Hiroyuki Kageyama, and Kuniaki Tatsumi

National Institute of Advanced Industrial Science and Technology (AIST), 1-8-31, Midorigaoka, Ikeda, Osaka 563-8577, Japan

Received January 15, 2005. Revised Manuscript Received June 28, 2005

By combining coprecipitation, hydrothermal, and firing methods under various firing temperatures (500−750 °C), Fe-substituted Li_2MnO_3 (nominal formula $Li_{1.2}Fe_{0.4}Mn_{0.4}O_2$) samples were prepared. A pure O3 phase was obtained below 700 °C. However, a small amount of spinel ferrite-like $LiFe_5O_8$ coexisted as an impurity phase for the sample that was fired at 750 °C. The maximum initial and 10th discharge capacities were obtained at 600−650 °C because of the balance between the development of 3d cation ordering, their primary particle size, and Li content, depending on the iron valence, which is changeable between 3+ and 4+.

1. Introduction

Positive electrode materials, including iron ion, have been studied energetically to forestall depletion of cobalt resources in $LiCoO_2$ with the development of large lithium-ion batteries. Although lithium iron phosphate ($LiFePO_4$) is a superior candidate as a 3 V positive electrode for that application, several valuable attempts have been made to find a 4 V positive electrode material based on complex lithium iron oxides. Those efforts have clarified the following. Although no 4 V plateau was observed on discharge for various $LiFeO_2$ phases[1−4] and although the discharge capacity of $LiFe_xM_{1-x}O_2$ ($0 < x < 0.3$, M = Co[5] and Ni[6]) decreases with Fe content, the Fe^{3+}/Fe^{4+} redox reaction appears around 4 V for solid solutions.[7,8] Delmas et al. proposed an explanatory model: the Fe^{4+} ion can be generated if it is surrounded only with Ni^{4+} (or Co^{4+}) ions.[8] However, no evidence exists indicating whether the Fe^{3+}/Fe^{4+} redox voltage exists at 4 V without the oxidation/reduction of other 3d elements. For that reason, Fe-substituted Li_2MnO_3 ($LiFeO_2-Li_2MnO_3$ solid solution: $Li_{(4-y)/3}Mn_{(2-2y)/3}Fe_yO_2$, $0 < y < 1$) was designed for extracting Fe^{3+}/Fe^{4+} redox voltage[9,10] because Li_2MnO_3 is known to be electrochemically inactive below 4.5 V. That ideal structure is shown in Figure 1. The Fe^{3+} ions can exist with Mn^{4+} ions on the 3b sites in the Fe−Mn−Li layers. The Fe-substituted Li_2MnO_3 was found to belong to a 4 V positive electrode material, as indicated by the appearance of the Fe^{3+}/Fe^{4+} redox voltage around 4 V.[9,10] Unfortunately, the specific capacity for $Li_{1.2}Fe_{0.4}Mn_{0.4}O_2$ is too small [70−80 (mA•h)/g even at a low current density of 7.5 mA/g] for practical use. Careful optimization of preparation conditions must be undertaken to overcome the problem. Preparation of a reactive precursor with complete mixing of 3d metal is especially important for Co-substituted $LiNi_{0.5}Mn_{0.5}O_2$[11,12] with better electrochemical performance. In fact, some improvement of the electrochemical properties [discharge capacity: >80 (m•Ah)/g] at typical current density (42 mA/g) is accomplished for our samples by selecting a reactive precursor with homogeneous Fe−Mn distribution.[13] However, effects of other preparation factors should be examined for further improvement of their electrochemical properties.

In this work, effects of firing temperature on electrochemical behavior were examined for 500−750 °C under an oxygen atmosphere using optimized deposition conditions

---

* Corresponding author. Tel.: +81-72-751-9618. Fax: +81-72-751-9714. E-mail address: m-tabuchi@aist.go.jp.

(1) Kanno, R.; Shirane, T.; Kawamoto, Y.; Takeda, Y.; Takano, M.; Ohashi, M.; Yamaguchi, Y. *J. Electrochem. Soc.* **1996**, *143* (8), 2435−2442.

(2) Sakurai, Y.; Arai, H.; Okada, S.; Yamaki, *J. Power Sources* **1997**, *68*, 711−715.

(3) Ado, K.; Tabuchi, M.; Kobayashi, H.; Kageyama, H.; Nakamura, O.; Inaba, Y.; Kanno, R.; Takagi, M.; Takeda, Y. *J. Electrochem. Soc.* **1997**, *144* (7), L177−L180.

(4) Tabuchi, M.; Nakashima, A.; Shigemura, H.; Ado, K.; Kobayashi, H.; Sakaebe, H.; Tatsumi, K.; Kageyama, H.; Nakamura, T.; Kanno, R. *J. Mater. Chem.* **2003**, *13*, 1747−1757.

(5) Alcántara, R.; Jumas, J. C.; Lavela, P.; Olivier-Fourcade, J.; Pérez-Vicente, C.; Tirado, J. L. *J. Power Sources* **1999**, *81−82*, 547−553.

(6) Reimers, J. N.; Rossen, E.; Jones, C. D.; Dahn, J. R. *Solid State Ionics* **1993**, *61*, 335−344.

(7) Kobayashi, H.; Shigemura, H.; Tabuchi, M.; Sakaebe, H.; Ado, K.; Kageyama, H.; Hirano, A.; Kanno, R.; Wakita, M.; Morimoto S.; Nasu, S. *J. Electrochem. Soc.* **2000**, *147*, 960−969.

(8) Delmas, C.; Ménétrier, M.; Croguennec, L.; Saadoune, I.; Rougier, A.; Pouillerie, C.; Prado, G.; Grüne, M.; Fournès, L. *Electrochim. Acta* **1999**, *45*, 243−253.

(9) Tabuchi, M.; Shigemura, H.; Ado, K.; Kobayashi, H.; Sakaebe, H.; Kageyama, H.; Kanno, R. *J. Power Sources* **2001**, *97−98*, 415−419.

(10) Tabuchi, M.; Nakashima, A.; Shigemura, H.; Ado, K.; Kobayashi, H.; Sakaebe, H.; Kageyama, H.; Kohzaki, M.; Hirano, A.; Kanno, R. *J. Electrochem. Soc.* **2002**, *149*, A509−A524.

(11) Jounneau, S.; Eberman, K. W.; Krause, L. J.; Dahn, J. R. *J. Electrochem. Soc.* **2003**, *150* (12), A1637−A1642.

(12) Park, S.-H.; Shin, H.-S.; Myung, S.-T.; Yoon, C. S.; Amine, K.; Sun, Y.-K. *Chem. Mater.* **2005**, *17*, 6−8.

(13) Tabuchi, M.; Nakashima, A.; Ado, K.; Sakaebe, H.; Kobayashi, H.; Kageyama, H.; Tatsumi, K.; Kobayashi, Y.; Yamanaka, A. Meeting abstract of IMLB-12, Nara, Japan, 2004; Abs. No. 160.

10.1021/cm050095+ CCC: $30.25

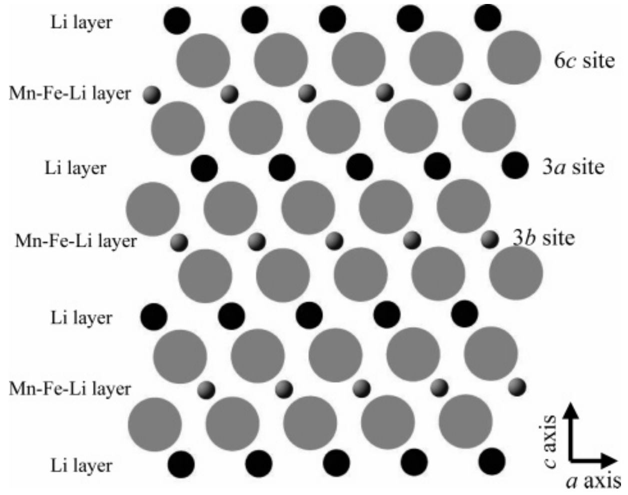

Figure 1. Crystal structure of Fe-substituted Li_2MnO_3 with ideal cation distribution on the *a*−*c* plane.

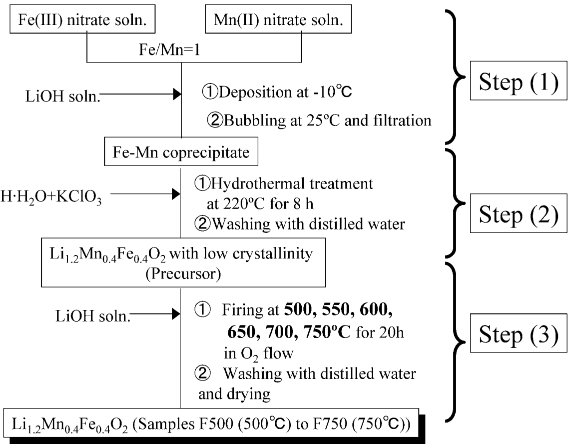

Figure 2. Synthetic route for Fe-substituted Li_2MnO_3. Samples F500−F750 were obtained by controlling the firing temperatures of 500−750 °C with 50 °C steps.

of Fe−Mn coprecipitate. Throughout this work, we attempt to determine why Fe-substituted Li_2MnO_3 ($Li_{1.2}Fe_{0.4}Mn_{0.4}O_2$) that is fired at 600−650 °C has maximum discharge capacity. The optimized firing temperature is considerably lower than those for $LiNi_{0.5}Mn_{0.5}O_2$ (>800 °C)[14] and other practical positive electrodes such as $LiCoO_2$ (>900°C), $LiNi_{0.8}Co_{0.2}O_2$ (>750 °C), and $LiMn_2O_4$ (>900 °C).

2. Experimental Section

Three steps are required for obtaining homogeneous $Li_{1.2}Fe_{0.4}Mn_{0.4}O_2$ samples (0.25 mol), as shown in Figure 2.

In step 1, Fe−Mn coprecipitates were prepared by slowly dropping LiOH solution (50 g of $LiOH \cdot H_2O$ (>98% purity) dissolved into 500 mL of distilled water) into a mixed Fe−Mn nitrate solution [0.125 mol of $Fe(NO_3)_3 \cdot 9H_2O$ (>99.9% purity) and $MnCl_2 \cdot 4H_2O$ (>99% purity) dissolved into 500 mL of distilled water and 200 mL of ethanol] at −10 °C. Ethanol was added to avoid freezing the solution. The obtained coprecipitates were subjected to aging under air bubbling for 2 days at room temperature. Filtration processing separated the Fe−Mn coprecipitates.

In step 2, low-crystallinity $Li_{1.2}Fe_{0.4}Mn_{0.4}O_2$ fine powder (precursor) was formed by hydrothermal treatment of the coprecipitates listed above with excess amounts of $LiOH \cdot H_2O$ (50 g) and $KClO_3$ (50 g, >99.5% purity) at 220 °C for 8 h. The precursor was purified by rinsing with distilled water and subsequent filtration and drying at 100 °C.

In step 3, the six final products (samples F500−F750) were obtained by firing the mixture of the precursor and additional $LiOH \cdot H_2O$ (0.25 mol) in temperatures of 500−750 °C under oxygen flow. Through rinsing with distilled water, filtration, and subsequent drying at 100 °C, products were separated from residual salts and used as samples.

Elemental analyses of Li, Fe, and Mn using inductively coupled plasma spectrometry estimated the sample compositions. Purity and cation distribution were checked by X-ray diffraction (XRD) measurement (Rotaflex RU-200B/RINT; Rigaku) using monochromatized Cu Kα radiation within the 2θ ranges of 10−125°. The diffraction angle was calibrated using silicon powder (SRM 640c) as an external standard. The RIETAN-2000 program[15] was used for structural refinement with X-ray Rietveld analysis. A split pseudo-Voigt profile function was selected for pattern fitting. The particle shape and average particle size were determined respectively by scanning electron microscopy (SEM) observation (JSM-6700F; JEOL) and BET specific surface area measurement (Monosorb; Quantachrome Instruments). The magnetic field dependence of magnetization was measured at 300 K using a vibrating sample magnetometer (VSM; Riken Denshi) for determination of trace magnetic impurities similar to spinel ferrite such as $LiFe_5O_8$ and $MnFe_2O_4$. For calibrating the magnetization, $(NH_4)_2Mn(SO_4)_2 \cdot 6H_2O$ was used as the standard material. The ^{57}Fe Mössbauer spectra were measured at 300 K. The α-Fe foil calibrates the velocity axis. Each spectrum was fitted using overlapped symmetric doublets having Lorentzian line shape with different quadrupole splitting (QS) values (QS = 0−1.8 mm/s) as a result of crystallographic site-sharing of iron with other cations (Li or Mn ions). Mosswin software was used for fitting it. The Mn K-edge X-ray absorption near-edge structure (XANES) spectrum was measured using a laboratory-type X-ray spectrometer (EXAC-820; Technos) in transmission mode at 293 K. Hydrothermally obtained $LiMnO_2$ (orthorhombic phase) and Li_2MnO_3 (monoclinic phase) were used as trivalent and tetravalent manganese reference materials, respectively.

Charge and discharge tests were undertaken using a positive electrode comprising the sample (20 mg), acetylene black (5 mg), and poly(tetrafluoroethylene) powder (0.5 mg) between 3.0 and 4.3 V against the negative Li metal electrode at a fixed current density (42 mA/g). That corresponds to a 1/3*C* rate for the ideal capacity [126 (mA·h)/g], as calculated by assuming that 0.4 Li was extracted electrochemically per the chemical formula $Li_{1.2}Fe_{0.4}Mn_{0.4}O_2$ because of the oxidation of all trivalent irons to tetravalent ones.

3. Results and Discussion

3.1. Phase Identification and Powder Analysis. Six samples were obtained by changing the firing temperature from 500 to 750 °C with 50 °C steps (Figure 2). They were respectively designated as samples F500−F750. Only the layered rock-salt form with α-$NaFeO_2$-type (O3) structure was detected on each XRD pattern, as shown in Figure 3a. Heat treatment above 800 °C engendered formation of O3 and cubic rock salt phases ($Fm\bar{3}m$) like α-$LiFeO_2$. An unindexed small peak around $2\theta = 21°$ for each pattern originates from sublattice ordering of Li and Mn in the transition-metal-containing layer, which is more characteristic in the end member Li_2MnO_3.[14] Lu et al. reported that these

---

(14) Lu, Z.; Beaulieu, L. Y.; Donaberger, R. A.; Thomas, C. L.; Dahn, J. R. *J. Electrochem. Soc.* **2002**, *149* (6), A778−A791.

(15) Izumi, F.; Ikeda, T. *Mater. Sci. Forum.* **2000**, *321−324*, 198−203.

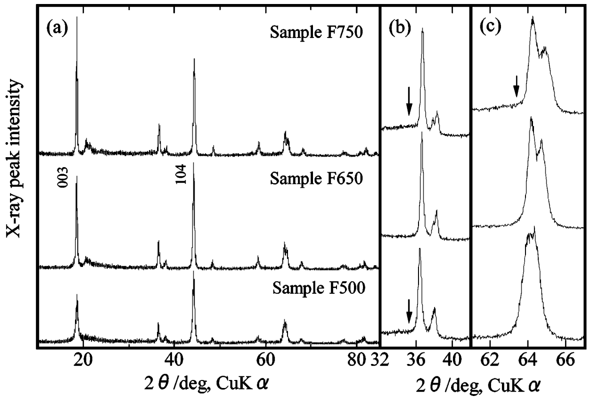

Figure 3. (a) XRD patterns for samples F500, F650, and F750 obtained respectively by firing precursor with LiOH at 500, 650, and 750 °C. The small difference between them is enhanced in parts b and c.

Table 1. Change in Chemical Composition as a Function of Firing Temperature[a]

sample	Li, wt %	Fe, wt %	Mn, wt %	Li/ (Fe + Mn)	Fe/ (Fe + Mn)
sample F500	8.51(5)	25.4(1)	24.5(1)	1.36(1)	0.50(1)
sample F550	8.70(1)	25.3(1)	24.5(1)	1.39(1)	0.50(1)
sample F600	9.27(9)	25.0(1)	24.2(1)	1.50(2)	0.50(1)
sample F650	9.64(8)	25.0(1)	24.3(1)	1.56(2)	0.50(1)
sample F700	9.80(2)	24.4(1)	23.8(1)	1.62(1)	0.50(1)
sample F750	9.16(8)	24.4(1)	24.1(1)	1.51(2)	0.50(1)
$Li_{1.2}Fe_{0.4}Mn_{0.4}O_2$	9.83	26.4	26.0	1.50	0.50

[a] The Li/(Fe + Mn) andFe/(Fe + Mn) ratios were estimated respectively as [(Li content)/6.94]/[(Mn content)/54.94 + (Fe content)/55.85] and [(Fe content)/55.85]/[(Mn content)/54.94 + (Fe content)/55.85]. Corresponding atomic weights of Li, Mn, and Fe are 6.94, 54.94, and 55.85, respectively. Ideal compositions of samples are shown for comparison.

small peaks result from random stacking of ordered sublattices along the *c* axis for NiO−Li_2MnO_3 solid solution, $Li[Ni_xLi_{1/3-2x/3}Mn_{2/3-x/3}]O_2$ ($0 < x < 1/2$)[14] with the same structure of Fe-substituted Li_2MnO_3. The Li, Mn, and Fe contents and Li/(Fe + Mn) and Fe/(Fe + Mn) ratios are listed in Table 1. Those values closely resemble the expected ones calculated from the chemical formula $Li_{1.2}Fe_{0.4}Mn_{0.4}O_2$. The preceding X-ray and elemental analyses demonstrate the successful formation of the target phase.

The powder character was verified through SEM observation analysis (Figure 4) and specific surface area (S_{BET}) measurements (Figure 5). All samples have agglomerate particles (1−20 μm not shown in Figure 4) comprising small primary particles with less than a 0.5-μm diameter. Although the primary particle size increased with firing temperature because of grain growth (Figure 4), that trend was not supported by the change in specific surface area (S_{BET}) as a function of firing temperature (Figure 5). The S_{BET} values decreased with firing temperature below 650 °C and increased beyond a 650 °C firing temperature. That anomaly might be explained by the difference in size of primary particles; extremely large primary particles with crystal habit above 1 μm coexist with small ones only for sample F650 (Figure 4b).

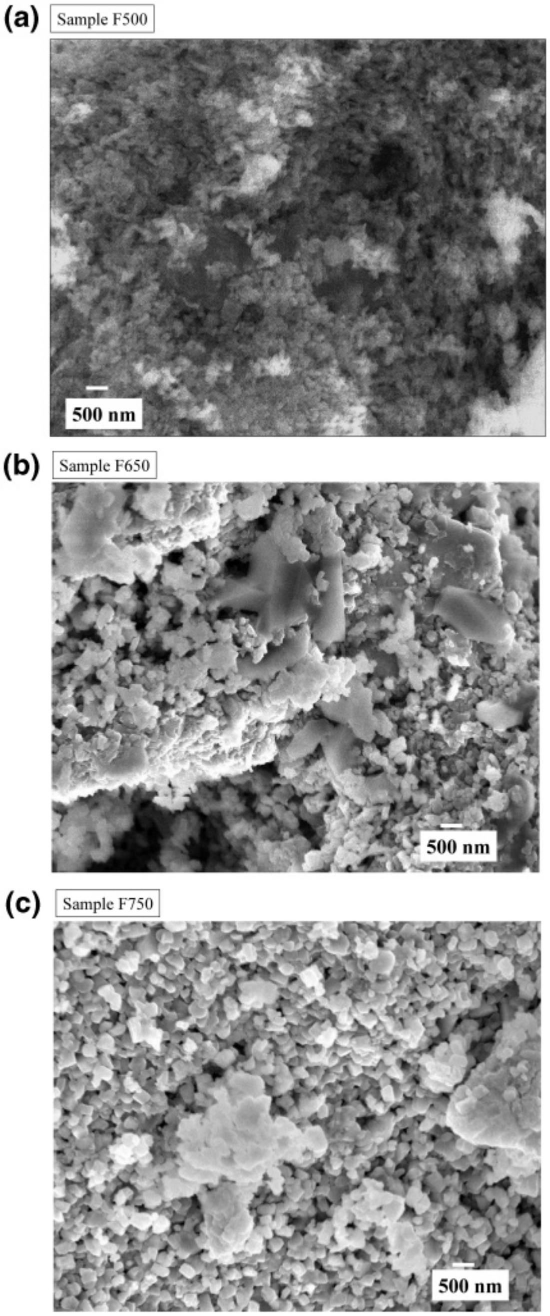

Figure 4. SEM photographs for primary particles of samples F500 (a), F650 (b), and F750 (c). Identical magnifications were selected for all samples.

3.2. Phase Purity Analysis through Magnetic Measurement. The XRD data for sample F750 were compared in detail to those of two other samples, F500 and F650, as shown in Figure 3b,c to detect small amounts of impurity. Broadened unknown peaks around $2\theta = 35-36°$ and 63° were observed for sample F750, and only the former one was detected for sample F500. The former and latter were indexed as 311 and 440 peaks, respectively, for spinel ferrites such as $LiFe_5O_8$ ($a = 8.333$ Å),[16] $MnFe_2O_4$ (Jacobsite, $a = 8.497$ Å),[17] or their solid solutions with inverse spinel structure ($Fd\bar{3}m$). To verify the presence of the spinel ferrites, magnetic field (*H*) dependence of magnetizations ($\sigma - H$ curve) were measured for all samples at 300 K (Figures 6 and 7) because they have spontaneous magnetization (σ_s) at 300 K originating from their ferrimagnetism below 943 K for $LiFe_5O_8$ [$\sigma_s = 65$ (G·cm^3)/g at 293 K][18] and 573 K for

---

(16) Schieber, M. *J. Inorg. Nucl. Chem.* **1964**, *26*, 1363−1367.
(17) Denecke, M. A.; Gunsser, W.; Baxbaum, G.; Kuske, P. *Mater. Res. Bull.* **1992**, *27*, 507−514.

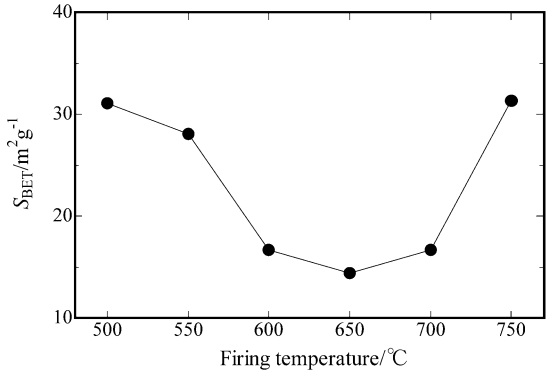

Figure 5. Change in specific surface area as a function of firing temperature.

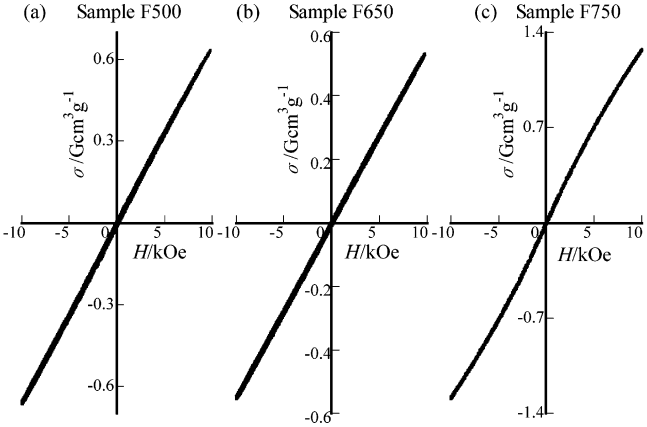

Figure 6. Magnetic field dependence of magnetization (σ) for samples F500 (a), F650 (b), and F750 (c) at 300 K.

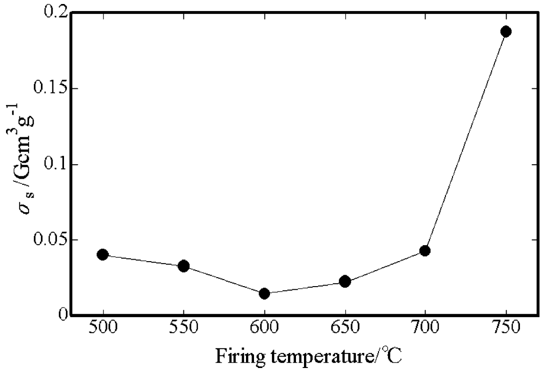

Figure 7. Change in spontaneous magnetization (σ_s) at 300 K as a function of firing temperature.

Table 2. X-ray Rietveld Refinement Results for (a) Samples F500 and (b) F650 Using a Layered Rock-Salt ($R\bar{3}m$) Unit Cell, $(Li_{1-m}M1_m)_{3a}[M2_nLi_{1-n}]_{3b}O_2$ ($0 < m < 1$, $0 < n < 1$), and (c, d) Sample F750 Using a Mixture of Layered Rock-Salt ($R\bar{3}m$) and Spinel Ferrite ($Fd3m$) Unit Cells[a]

atom	site	*g*	*x*	*y*	*z*	*B*, Å^2
		(a) Sample F500[b]				
Li/M1	3a	0.9131/0.0869(14)	0	0	0	1
M2/Li	3b	0.637(3)/0.363	0	0	1/2	0.5
O	6c	1	0	0	0.24311(15)	1
		(b) Sample F650[c]				
Li/M1	3a	0.9390/0.0610(14)	0	0	0	1
M2/Li	3b	0.651(3) /0.349	0	0	1/2	0.5
O	6c	1	0	0	0.24276(14)	1
		(c) Sample F750 Layered Rock Salt[d,e] (Mass Fraction: 88.03%)				
Li/M1	3a	0.9670/0.0330(16)	0	0	0	1
M2/Li	3b	0.659(4)/0.341	0	0	1/2	0.5
O	6c	1	0	0	0.24257(14)	1
		(d) Sample F750 Spinel Ferrite ($LiFe_5O_8$ Unit Cell, Mass fraction: 11.97%)[d,f]				
M1	8a	1	1/8	1/8	1/8	0.5
M2/Li	16d	0.75/0.25	1/2	1/2	1/2	0.5
O	32e	1	0.266(2)	$= x$	$= x$	1

[a] Both M1 and M2 correspond to Fe and/or Mn atoms. [b] $a = 2.8936(3)$ Å, $c = 14.3136(13)$ Å, $R_{wp} = 10.26\%$, $R_p = 7.76\%$, $S = 1.39$, $R_I = 3.37\%$, $R_F = 2.53\%$. [c] $a = 2.8803(2)$ Å, $c = 14.2841(10)$ Å, $R_{wp} = 12.13\%$, $R_p = 8.92\%$, $S = 1.48$, $R_I = 3.22\%$, $R_F = 2.89\%$. [d] $R_{wp} = 10.43\%$, $R_p = 7.79\%$, $S = 1.33$. [e] $a = 2.8845(2)$ Å, $c = 14.2788(10)$ Å, $R_I = 2.27\%$, $R_F = 2.08\%$. [f] $a = 8.390(14)$ Å, $R_I = 1.23\%$, $R_F = 1.38\%$.

$MnFe_2O_4$ [$\sigma_s = 80$ (G·cm^3)/g at 293 K].[18] The $\sigma-H$ curves for samples F500 and F650 looked like lines with positive gradients (Figure 6a,b), whereas that for sample F750 looked like an ogive (Figure 6c), indicating that magnetic impurity coexisted with paramagnetic $Li_{1.2}Fe_{0.4}Mn_{0.4}O_2$, which will be confirmed later through analysis of ^{57}Fe Mössbauer spectra. The observed σ_s values were 0.0405(12), 0.0227(11), and 0.1875(18) (G·cm^3)/g respectively for samples F500, F650, and F750, which were calculated as average ones between two absolute σ_s values estimated by extrapolating least-squares-fitted $\sigma-H$ data to a zero magnetic field within +7 to +10 kOe or −7 and −10 kOe. Sample F750 contained more magnetic impurity than the other two samples. Figure 7 shows that such a high σ_s value [>0.1 (G·cm^3)/g] was observed only for sample F750, fired at 750 °C. The estimated mass fraction of magnetic impurity for sample F750 was 0.29 or 0.23% if the impurity was only $LiFe_5O_8$ or $MnFe_2O_4$ and both exhibited bulk magnetism in this sample. The $LiFe_5O_8$ impurity contents for samples F500 and F650 were estimated respectively as 0.063 and 0.035%, if only $LiFe_5O_8$ coexisted with the O3 phase. On the basis of these magnetization data, the XRD pattern for sample F750 was fitted by a two-phase structural model of O3 and inverse spinel unit cells, whereas those for other samples were fitted by only the O3 phase model (Figure 8 and Tables 2 and 3). An attempt to fit the XRD pattern using the two-phase model failed for sample F500 because of the lack of improvement of the fitting parameters, R_{wp} (10.43%) and S (goodness of fit, 1.41), both of which were larger than those of the O3 phase model (10.26% and 1.39, see Table 2). A two-phase model was accepted only for sample F750 because both fitting parameters, R_{wp} and S, were reduced to 10.43% and 1.33 compared to 12.54% and 1.60 obtained from the single O3 phase model. The formed spinel ferrite is considered to be $LiFe_5O_8$ on the basis of the fact that the lattice parameter [8.390(14) Å] was nearly equal to that of $LiFe_5O_8$ (8.333 Å). The estimated mass fraction of $LiFe_5O_8$ was 11.97% (Table 2d), which is much larger than that from the magnetization data (0.3%). The large difference might be attributable to the broad-peak nature of ferrite, which is difficult to distinguish from the background. Therefore, the actual ferrite content might be less than 12%. Both magnetization and XRD data support that sample F750 is not a pure O3 phase but a mixture of O3 and $LiFe_5O_8$ phases.

3.3. Cation Distribution Analysis through X-ray Rietveld Analysis. Structural refinement of the O3 phase can detect the change in cation ordering and valence states of iron and manganese ions (Figures 8 and 9 and Table 3). The

---

(18) Smit, J.; Wijn, H. P. J. *Ferrites*; Philips Technical Library: Eindhoven, The Netherlands, 1965; p 157.

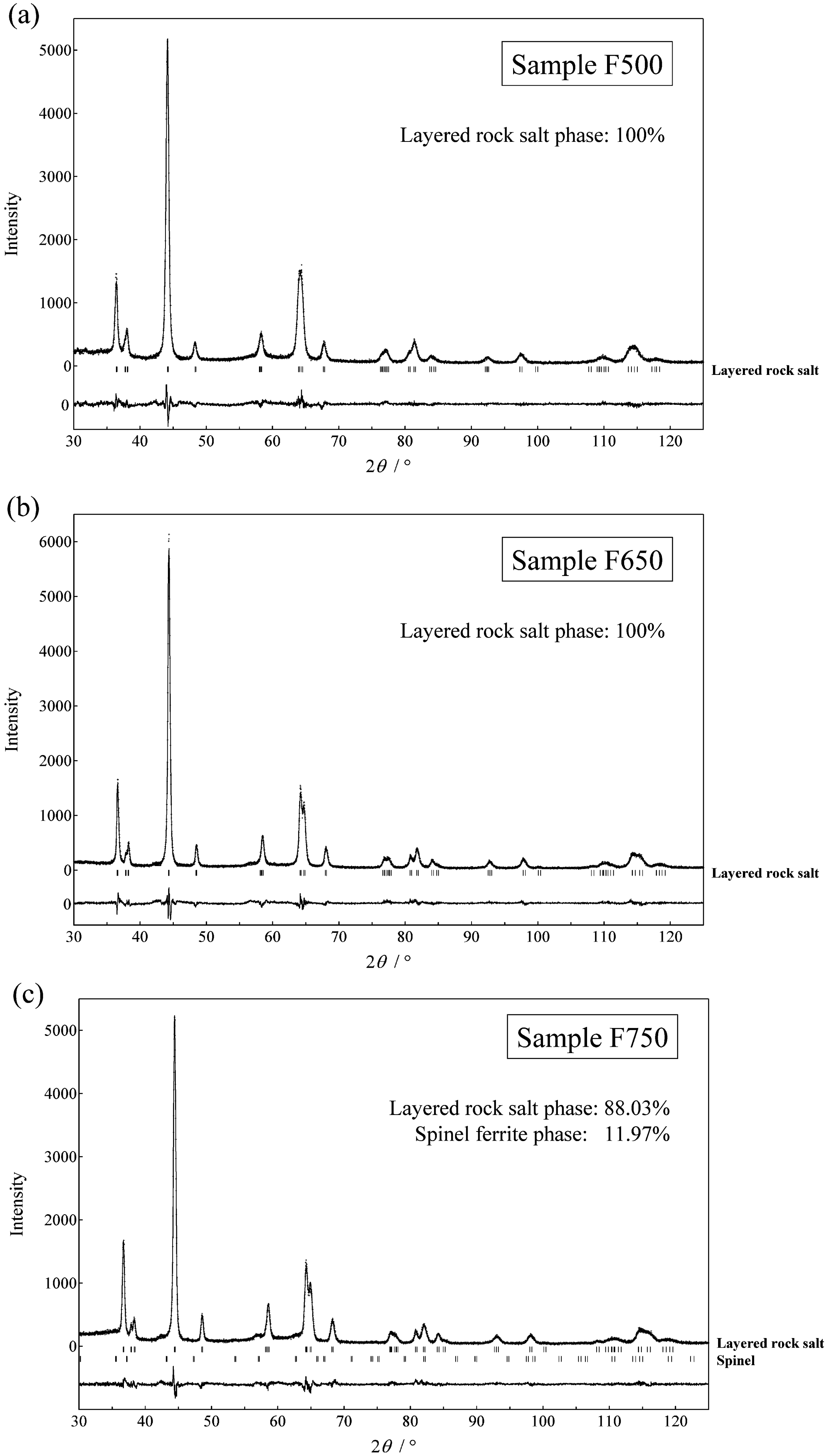

Figure 8. Observed (+) and calculated (solid line) XRD patterns for samples F500 (a), F650 (b), and F750 (c). The difference between the observed and the calculated data is given at the bottom of the figure with the same scale. Peak positions of layered rock-salt and spinel phases are expressed as vertical lines.

Table 3. Structural Parameters Using the Layered Rock-Salt Unit Cell ($R\bar{3}m$), $(Li_{1-m}M1_m)_{3a}[M2_nLi_{1-n}]_{3b}O_2$ ($0 < m < 1$, $0 < n < 1$)[a]

sample	firing temperature/°C	a, Å	c, Å	$100g_{3a}$, %	$100g_{3b}$, %	$100(g_{3a} + g_{3b})$, %	R_{wp}, %	S
sample F500	500	2.8936(3)	14.3136(13)	8.69(14)	63.7(3)	72.4(3)	10.26	1.39
sample F550	550	2.8904(3)	14.3042(12)	8.25(14)	63.6(2)	71.9(2)	10.46	1.40
sample F600	600	2.8821(3)	14.2792(10)	6.67(13)	64.4(2)	71.1(2)	11.02	1.38
sample F650	650	2.8803(2)	14.2741(10)	6.10(14)	65.1(3)	71.2(3)	12.13	1.48
sample F700	700	2.8835(3)	14.2985(11)	4.50(15)	66.0(3)	70.5(3)	12.85	1.68
sample F750[b]	750	2.8745(2)	14.2788(10)	3.30(16)	65.9(4)	69.2(4)	10.43	1.33

[a] Occupancies of 3d metal ions on 3a and 3b sites (g_{3a} and g_{3b}) correspond respectively to the m and n values in the above structural model. [b] Spinel ferrite (probably $LiFe_5O_8$) was contained in this sample as a minor second phase (12% mass fraction).

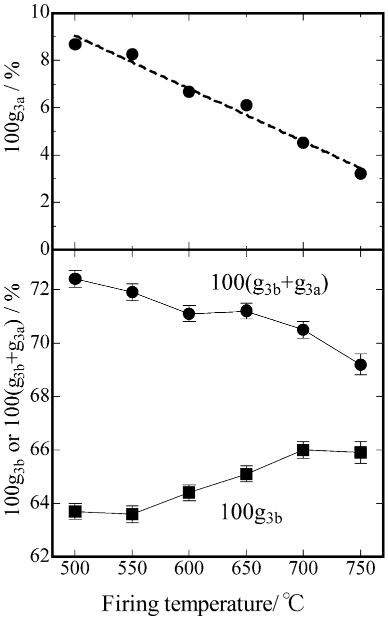

Figure 9. Change in occupancy of transition metals on 3a and 3b sites (g_{3a} and g_{3b}, respectively), and their sum ($g_{3a} + g_{3b}$) as a function of firing temperature.

cation distribution model was $(Li_{1-m}M1_m)_{3a}[M2_nLi_{1-n}]_{3b}O_2$ ($0 < m < 1$, $0 < n < 1$). Both M1 and M2 correspond to Fe and/or Mn atoms existing on 3a (000) and 3b (00$^1/_2$) sites, respectively (Figure 1). Selected refinement parameters are listed in Table 3. The m and n values correspond to the occupancy of Fe and/or Mn ions on 3a (g_{3a}) and 3b (g_{3b}) sites, respectively; the former parameter decreased and the latter one increased with increasing firing temperatures between 550 and 700 °C, reflecting the 3d cation ordering to the 3b site (Figure 9). The increase in the g_{3b} (n) value ceased, but the g_{3a}(m) value decreased by firing at 750 °C. The result is considered to be extraction of Fe ions from O3 structure because of sample decomposition to a mixture of O3 (Fe/Mn < 1) and $LiFe_5O_8$ phases.

3.4. Valence State Analyses through Mn K-Edge X-ray Absorption and ^{57}Fe Mössbauer Spectroscopy.

Figure 9 shows that the total amount of Mn and Fe ions, the $m + n$ value, decreased with firing temperature up to 700 °C, indicating that some factor aside from sample decomposition must be taken into account. The $m + n$ value is sensitive to change in the valence states of Mn and Fe; the lowering of the $m + n$ value can be accomplished by oxidation of either Mn^{4+} or Fe^{3+} with incorporation of Li into the O3 structure. In fact, the Li/(Fe + Mn) ratio increased with increasing firing temperature, as shown in Table 1. The Mn K-edge XANES spectra for samples F500, F600, and F700 were mutually similar in shape and energy position and nearly overlapped with that of the end member Li_2MnO_3 (Figure 10) that was selected as a standard material of tetravalent manganese oxide. No change was detected in the manganese oxidation state.

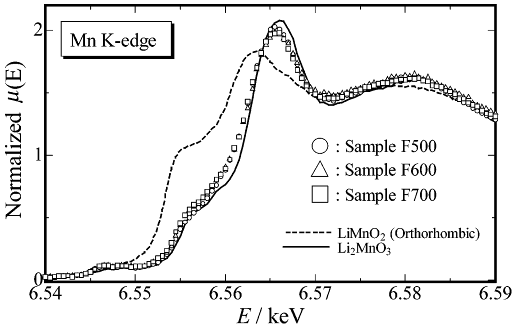

Figure 10. Mn K-edge XANES spectra for samples F500, F600, and F700 with those of two standard materials: orthorhombic $LiMnO_2$ and monoclinic Li_2MnO_3 obtained by hydrothermal reaction.

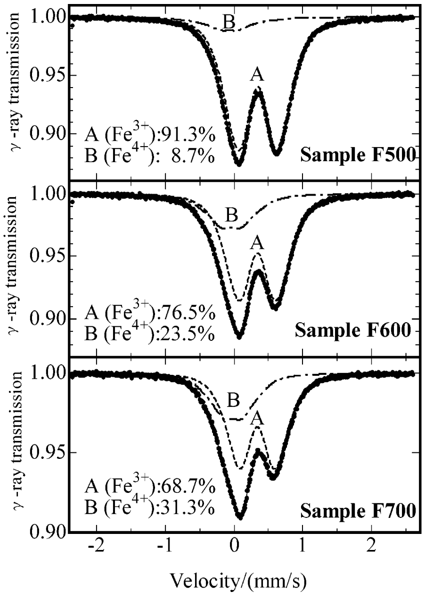

Figure 11. Observed (●) and calculated (solid line) ^{57}Fe Mössbauer spectra for samples F500, F600, and F700 at 300 K. Two symmetric doublets with different IS values were denoted as A and B components and used for constructing the calculated spectra. The area fractions of individual components are shown in this figure.

The ^{57}Fe Mössbauer spectra for samples F500, F600, and F700 were fitted by two symmetric doublets with different isomer shift (IS) values (IS = +0.3 and 0 mm/s) because of their asymmetric shape (Figure 11). The "A" and "B" components were assigned as Fe^{3+} in a high-spin configuration and Fe^{4+} ones based on previous data for $Li_x(Ni_{0.9}Fe_{0.1})_{1.06}O_2$ ($x = 0.94$ and 0.28) with O3 structure[8,19] and other lithium transition metal oxides with rock-salt-related structure including the high-spin Fe^{3+} ion,[4,20,21] as listed in Table 4.

Table 4. ^{57}Fe Mössbauer Parameters at 300 K for Samples F500−F750 with Standard Materials with Rock-Salt-Related Structures

sample	crystal structure	component (area ratio)	IS, mm/s	QS,[a] mm/s
sample F500	layered rock salt ($R\bar{3}m$)	A (Fe^{3+}, 91.3%)	+0.3449(3)	0.582(16)
		B (Fe^{4+}, 8.7%)	−0.072(4)	0.31(2)
sample F550	layered rock salt ($R\bar{3}m$)	A (Fe^{3+}, 87.5%)	+0.3428(5)	0.573(11)
		B (Fe^{4+}, 12.5%)	−0.057(4)	0.306(13)
sample F600	layered rock salt ($R\bar{3}m$)	A (Fe^{3+}, 76.5%)	+0.3398(4)	0.558(11)
		B (Fe^{4+}, 23.5%)	−0.043(4)	0.32(2)
sample F650	layered rock salt ($R\bar{3}m$)	A (Fe^{3+}, 73.1%)	+0.3378(4)	0.548(11)
		B (Fe^{4+}, 26.9%)	−0.020(4)	0.34(2)
sample F700	layered rock salt ($R\bar{3}m$)	A (Fe^{3+}, 68.7%)	+0.3390(6)	0.526(12)
		B (Fe4+, 31.3%)	−0.018(5)	0.305(19)
sample F750	layered rock salt ($R\bar{3}m$)	A (Fe^{3+}, 73.8%)	+0.3405(6)	0.525(11)
		B (Fe^{4+}, 26.2%)	−0.037(3)	0.314(16)
$Li_{0.94}(Ni_{0.9}Fe_{0.1})_{1.06}O_2$ (refs 8 and 19)	layered rock salt	A (Fe^{3+}, 100%)	+0.33	0.33(3)
$Li_{0.28}(Ni_{0.9}Fe_{0.1})_{1.06}O_2$ (refs 8 and 19)	layered rock salt ($R\bar{3}m$)	A (Fe^{3+}, 54%)	+0.33	0.8(3)
		B ($Fe^{3.5+}$, 36%)	+0.20	0.5(2)
		C (Fe^{4+}, 10%)	−0.11	1.1(5)
layer−$LiFeO_2$ (ref 20)	layered rock salt ($R\bar{3}m$)	A (Fe^{3+}, 100%)	+0.35	0.34
$LiCo_{0.8}Fe_{0.2}O_2$ (ref 21)	layered rock salt ($R\bar{3}m$)	A (Fe^{3+}, 100%)	+0.3213(3)	0.31(4)
α-$LiFeO_2$ (ref 4)	cubic rock salt ($Fm\bar{3}m$)	A (Fe^{3+}, 100%)	+0.361(1)	0.60(4)
$Li_{1.2}Fe_{0.4}Ti_{0.4}O_2$ (ref 4)	cubic rock salt ($Fm\bar{3}m$)	A (Fe^{3+}, 100%)	+0.358(1)	0.62(5)

[a] Each spectrum of samples F500−F750 was fit by two QS distributed doublets. The QS distribution analysis was performed between 0 and 1.8 mm/s with a fixed line width, 0.2 mm/s for the "A" component and between 0 and 1.5 mm/s with a fixed line width, 0.3 mm/s for the "B" component.

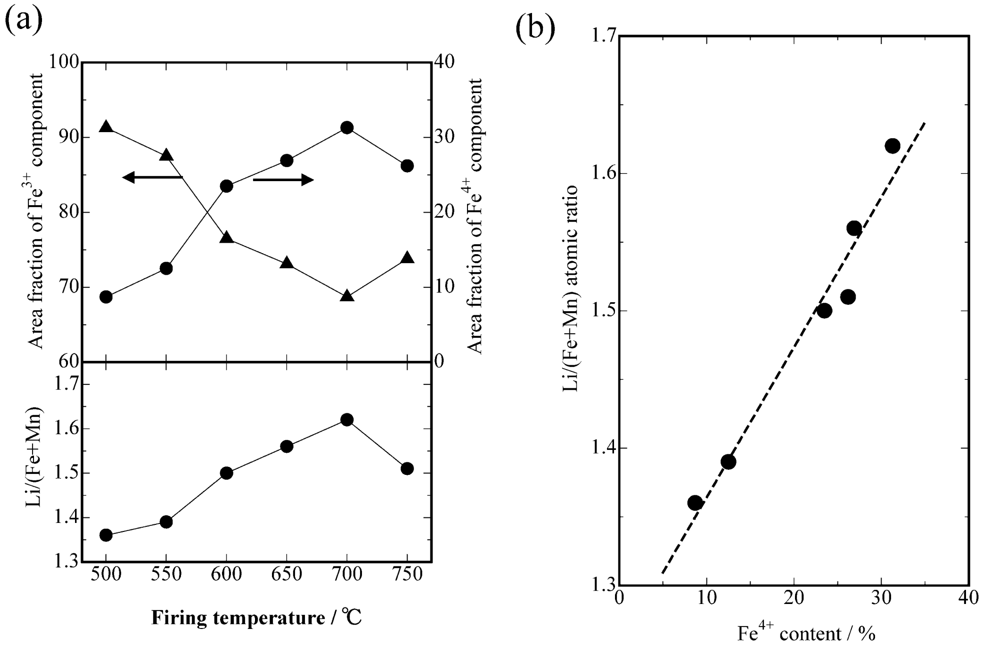

Figure 12. (a) Change in area fractions of Fe^{3+} and Fe^{4+} components estimated from ^{57}Fe Mössbauer spectra at 300 K and in lithium to 3d metal atomic ratios as a function of firing temperature. In part b, area fractions of Fe^{4+} components are plotted against lithium to 3d metal atomic ratios; the broken line is a least-squares fitting line between these parameters.

Only the high-spin Fe^{3+} component was observed for a hydrothermally obtained sample given at step 2 in Figure 2. The Fe^{4+} component appeared after firing; its area fraction increased to 700 °C and decreased beyond 700 °C with increasing firing temperature (Figure 12a, upper). The change in the ^{57}Fe Mössbauer spectra showed that Fe ions in $Li_{1.2}Fe_{0.4}Mn_{0.4}O_2$ were oxidized to 700 °C and reduced at temperatures greater than 700 °C, which can explain the decrease in $m + n$ ($g_{3a} + g_{3b}$) values below 700 °C.

The tendency of Fe^{4+} content is similar to that of the Li/(Mn + Fe) ratio against firing temperature, as shown in the bottom part of Figure 12a. The Li/(Mn + Fe) ratio value increased linearly with Fe^{4+} content (Figure 12b), indicating that incorporation of Li into $Li_{1.2}Fe_{0.4}Mn_{0.4}O_2$ was governed mainly by the degree of oxidation of Fe^{3+} ions. The change in the chemical formula is given as

$$Li_{(4-y)/3}Mn^{4+}{}_{(2-2y)/3}Fe^{3+}{}_{y}O_2\ (y = 0.4) \rightarrow$$
$$Li_{(4-z)/3}(Mn^{4+}, Fe^{4+})_{(2-2z)/3}Fe^{3+}{}_{z}O_2\ (z < 0.4)$$

The QS distribution of each symmetric doublet was compared with those of other compounds with layered and cubic rock-salt structures to elucidate which of the Fe ions with 3+ or 4+ oxidation states exist in the Li layer (3a site). In our previous report, only Fe ions existed at both 3a and

---

(19) Prado, G.; Rougier, A.; Fournes, L.; Delmas, C. *J. Electrochem. Soc.* **2000**, *147*, 2880−2887.

(20) Tabuchi, M.; Ado, K.; Kobayashi, H.; Matsubara, I.; Kageyama, H.; Wakita, M.; Tsutsui, S.; Nasu, S.; Takeda, Y.; Masquelier, C.; Hirano, A.; Kanno, R. *J. Solid State Chem.* **1998**, *141*, 554−561.

(21) McLaren, V. L.; West, A. R.; Tabuchi, M.; Nakashima, A.; Takahara, H.; Kobayashi, H.; Sakaebe, H.; Kageyama, H.; Hirano, A.; Takeda, Y. *J. Electrochem. Soc.* **2004**, *151* (5), A672−A681.

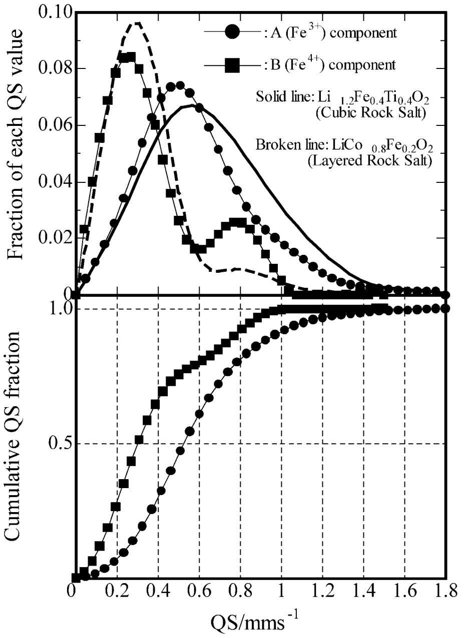

Figure 13. QS distributions for two symmetric doublets of ^{57}Fe Mössbauer spectra for sample F700. Distributions of two rock-salt related solid solutions with different Fe ion arrangements are plotted for comparison in the upper figure. In the lower figure, cumulative QS distribution curves of these components are plotted to portray their large difference in average QS data.

3b sites.[10] The QS distribution results from interaction between a focused ^{57}Fe nuclei and electronic field gradient originated from adjacent oxide anion and cations.[22] Its QS distribution would be extended to a higher QS value because of the difference in local cation distribution between the two sites[22] if focused Fe ions simultaneously occupied two different crystallographic (3a and 3b) sites. Large differences in QS distribution between the two doublets was observed as an example of sample F700; the distribution for the A (Fe^{3+}) component was extended to a higher QS value than that for the B (Fe^{4+}) component (Figure 13). Although the QS distributions of the Fe^{4+} component were almost equal to that for $LiCo_{0.8}Fe_{0.2}O_2$ (broken curve) with layered rock-salt structures, the other one was close to $Li_{1.2}Fe_{0.4}Ti_{0.4}O_2$ with cubic rock-salt structure (solid curve) rather than that for $LiCo_{0.8}Fe_{0.2}O_2$. The cubic rock salt structure can be considered as a complete cation disordered one of layered rock-salt structure. Therefore, only Fe^{3+} ion seems to exist at both 3a and 3b sites without site preference. To confirm this and for comparing the distributed QS data to the previous one, the average QS value was calculated by transformation to a cumulative QS distribution, as shown in the bottom part of Figure 13. The objective value was a point at the intersection of cumulative QS distribution curve with a horizontal line at 0.5 of the cumulative QS value. A regression line using cumulative QS fraction data between 0.3 and 0.7 approximated the cumulative QS distribution curve. The average QS values for A and B components are listed in Table 4. The former one is close to those for α-$LiFeO_2$ and $Li_{1.2}Fe_{0.4}Ti_{0.4}O_2$; the latter one is close to those for layer−$LiFeO_2$ and $LiCo_{0.8}Fe_{0.2}O_2$. The QS distribution analysis suggests that only trivalent irons exist at both 3a and 3b sites. The average QS data would increase with increasing occupancy of 3*d* cations on the 3*a* site if QS distribution data of the A (Fe^{3+}) component were influenced by the mode of cation distribution. The average QS data were plotted against the occupancy values (Figure 14). The average QS data for the A component decreased with decreasing cation disordering, whereas that for the B component was independent: only Fe^{3+} ions exist at both sites. The result is reasonable considering the structural character of the O3 phase because the nearest metal ion at the 3*a* site, with oxide ion distances of 2.10 Å, is larger than that at the 3b site, with oxide ion distances of 1.98 Å (see Figure 1), and larger Fe^{3+} ions (0.645 Å) than the Fe^{4+} one (0.585 Å) can be stabilized at the 3a site. The QS distribution analysis is an important tool for characterizing Fe ion distribution because X-ray Rietveld analysis cannot distinguish what kind of 3d ions exist on the 3a site when a third 3d element like Ni or Co is added for improving their electrochemical properties.

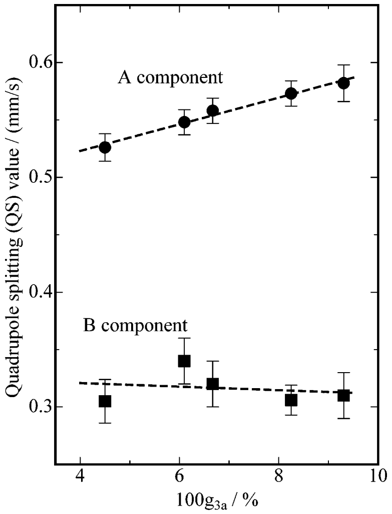

Figure 14. Relation between two sets of QS data and occupancy of 3d metal ion at a 3a site in the Li layer. The broken line is a least-squares fitting line between the QS values and occupancy.

3.5. Charge and Discharge Characteristics. Comparison of charge and discharge curves among three samples (samples F500, F650, and F750, Figure 15) shows the sensitivity of the electrochemical property to firing temperature. (1) Initial charge and discharge capacities were smallest for the Li/sample F750 cell among the three cells. (2) Average voltages of initial discharge curves increased with increasing firing temperature from the Li/sample F500 (3.70 V) to the Li/sample F750 (3.85 V). (3) The 10th discharge capacity above 3.5 V ($Q_{10d3.5}$) for the Li/sample F650 cell was larger than for the other two cells. The initial and 10th discharge capacities were plotted against firing temperature (Figure 16). All discharge capacities decreased at temperatures greater than 650 °C. The initial discharge capacities above 3.0 V ($Q_{1d3.0}$) and 3.5 V ($Q_{1d3.5}$) for the Li/sample F750 cell were smallest among all cells, whereas the discharge capacity retention above 3.5 V after the 10th cycle ($Q_{10d3.5}/Q_{1d3.5}$) was higher than for the other cells. Electrochemical data showed the optimum firing temperature as 600−650 °C for $Li_{1.2}Fe_{0.4}Mn_{0.4}O_2$, which is lower than other typical positive electrodes.

---

(22) Waerenborth, J. C.; Figuriredo, F. M.; Frade, J. R.; Colomer, M. T.; Jurado, J. R. *J. Phys.: Condens. Matter* **2001**, *13*, 8171−8187.

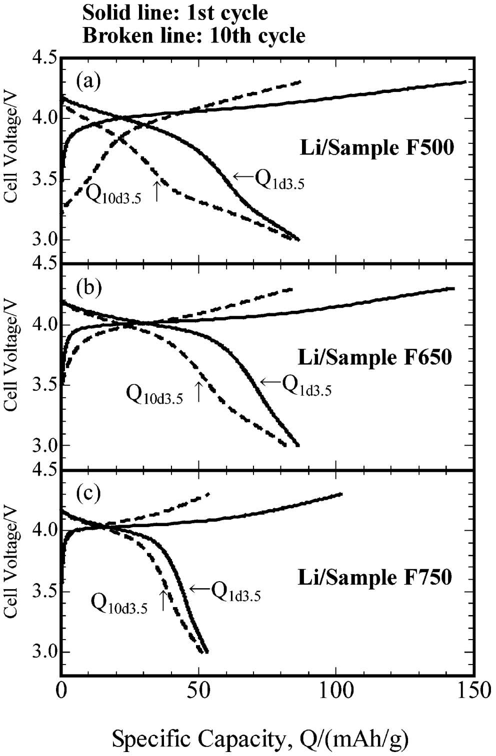

Figure 15. Initial and 10th charge−discharge curves of three Li/sample cells. Arrows indicate the 1st and 10th discharge capacities above 3.5 V, designated as $Q_{1d3.5}$ and $Q_{10d3.5}$.

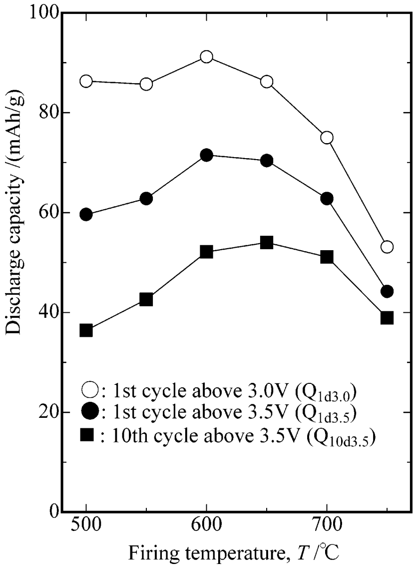

Figure 16. Change in discharge capacities as a function of firing temperature.

4. Factors for Determining the Discharge Capacity of Fe-Substituted Li_2MnO_3 Greater than 3.5 V

This section examines the origin of appearance of optimum heat-treatment temperature for electrochemical behavior. Figure 17 summarizes our obtained results. Eight factors were considered. Among them, only Mn valence was unchanged at 4+ throughout our experimental condition. Therefore, this factor can be excluded from consideration.

<table>
<tr><td>Sample</td><td>F500</td><td>F550</td><td>F600</td><td>F650</td><td>F700</td><td>F750</td></tr>
<tr><td>F.T./℃</td><td>500</td><td>550</td><td>600</td><td>650</td><td>700</td><td>750</td></tr>
<tr><td>1st discharge capacity above 3.5 V</td><td colspan="2">Increased</td><td colspan="2">Maximum</td><td colspan="2">Decreased</td></tr>
<tr><td>10th discharge capacity above 3.5 V</td><td colspan="2">Increased</td><td colspan="3">Maximum</td><td>Decreased</td></tr>
<tr><td>Primary particle size</td><td colspan="6">Increased</td></tr>
<tr><td>Specific surface area</td><td colspan="3">Decreased</td><td>Minimum</td><td colspan="2">Increased</td></tr>
<tr><td>Observed phase</td><td colspan="5">Layered rock-salt only</td><td>Layered rock salt + spinel</td></tr>
<tr><td>Magnetic impurity</td><td colspan="5">Difficult to detect</td><td>Clearly detected</td></tr>
<tr><td>Li/(Fe+Mn)</td><td colspan="4">Increased</td><td>Maximum</td><td>Decreased</td></tr>
<tr><td>Fe ion ordering</td><td colspan="4">Increased</td><td>Maximum</td><td>----------</td></tr>
<tr><td>Fe valence</td><td colspan="4">Partially Oxidized from 3+ to 4+</td><td>Maximum</td><td>Reduced</td></tr>
<tr><td>Mn valence</td><td colspan="6">Kept at 4+</td></tr>
</table>

Figure 17. Summary of this work for constructing the relation between discharge capacity and firing temperature. "Increased", "Decreased", "Oxidized", and "Reduced" were used to denote changes in respective parameters with increasing firing temperature.

As mentioned, initial and 10th discharge capacities above 3.5 V were increased with firing temperature for samples fired below 650 °C. Grain growth of particles, Fe ion ordering to the 3b site, and incorporation of Li ion into the structure by oxidation of Fe ion were also observed. Development of Fe ion ordering is preferable for better electrochemical performance for two reasons: (1) Fe ions on the 3a site can act as blocking ions for fast Li diffusion during charge−discharge reactions as well as other O3 positive electrodes such as $LiNiO_2$[23] or $LiNi_{0.8}Co_{0.2}O_2$;[24] and (2) only Fe ions neighboring Mn^{4+} ions on the 3b site can participate in electrochemical reactions[10] like Fe-substituted $LiNiO_2$.[8,19] The cation ordering effect might be predominant over the change in chemical formula from $Li_{(4-y)/3}Mn_{(2-2y)/3}Fe_yO_2$ ($y = 0.4$) to $Li_{(4-z)/3}(Mn^{4+}, Fe^{4+})_{(2-2z)/3}Fe^{3+}_zO_2$ ($z < 0.4$), which can degrade their electrochemical performance because of the decreasing Fe^{3+} ion content.

The discharge capacity was lower at firing temperatures above 700 °C. Three possible reasons are (i) decomposition of the sample caused by formation of spinel ferrite ($LiFe_5O_8$), (ii) decreasing Li content because of reduction of Fe^{4+} ion, and (iii) increasing primary particle size. The coexistence of $LiFe_5O_8$ would reduce the charge and discharge capacities of sample F750 because $LiFe_5O_8$ is an electrochemically inactive phase within the present charge−discharge voltage range. Furthermore, iron content in the O3 phase was reduced because of the formation of such Fe-rich oxides. If $LiFe_5O_8$ grew on the surface of the O3 phase, it would hinder the electrochemical extraction and insertion reactions, even if its content were low. A previous report included the deduction that $LiCr_xFe_{5-x}O_8$ ($x = 0.25$) overgrew on the surface of an Fe-substituted $LiCrO_2$ single crystal.[25] Therefore, spinel ferrite formation is a possible degradation mechanism for Fe-substituted Li_2MnO_3.

The contribution of factor (i) to capacity degradation was judged using Al-substituted samples because they retain small magnetic impurity contents throughout our experimental conditions. The samples were obtained by adding aluminum

---

(23) Arai, H.; Okada, S.; Otsuka, H.; Ichimura, M.; Yamaki, J. *Solid State Ionics* **1995**, *80*, 261−269.

(24) Gover, R.; Kanno, R.; Mitchell, B.; Yonemura, M.; Kawamoto, Y. *J. Electrochem. Soc.* **2000**, *147* (11), 4045−4051.

(25) Tauber, A.; Moller, W. M.; Banks, E. *J. Solid State Chem.* **1972**, *4*, 138−152.

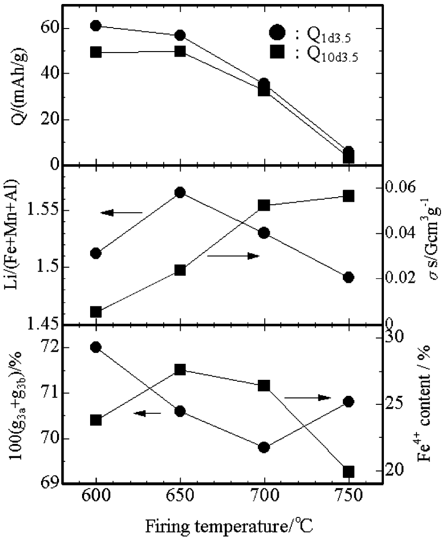

Figure 18. Change in discharge capacities ($Q_{1d3.5}$ and $Q_{10d3.5}$), atomic ratio of lithium to the sum of other cations Li/(Fe + Mn + Al), spontaneous magnetization σ_s, sum of Fe and Mn occupancies on both 3a and 3b sites $g_{3a} + g_{3b}$, and the area fraction of Fe^{4+} component as a function of firing temperature.

nitrate solution with lithium hydroxide to hydrothermally obtained precursor in step 3 (see Figure 2). The elemental analysis indicated that 2.5 mol % of Al was incorporated per sum of all cation contents except for Li. We prepared four samples by changing the firing temperature between 600 and 750 °C. Our XRD data analysis revealed the formation of pure O3 phase. An increase in the primary particle size was detected by SEM observation with increased firing temperatures of 600−750 °C. Figure 18 shows that the initial and 10th discharge capacities for Al-substituted samples decreased drastically by firing them at temperatures greater than 650 °C from 50 (mA·h)/g to less than 10 (mA·h)/g, whereas no drastic change in spontaneous magnetization (σ_s) or sum of 3d metal occupation [$100(g_{3a} + g_{3b})$] was detected. These results reveal that the iron loss attributable to the spinel ferrite formation (factor i) is not responsible for capacity degradation. Both the Li/(Al + Fe + Mn) ratio and Fe^{4+} content decreased at firing temperatures above 650 °C. The temperature dependency of each parameter is consistent with the capacity trend. The observation for Al-substituted samples cannot exclude the contribution of factors (ii) and (iii) as possible reasons for high-temperature capacity degradation. A preparation route of Fe-substituted Li_2MnO_3 must be established for practical use of this positive electrode. It must yield a small primary particle size (<100 nm) while retaining a highly cation-ordered structure with high Fe^{4+} content.

5. Conclusions

Effects of firing temperature on electrochemical properties of Fe-substituted Li_2MnO_3 samples were clarified through analyses of their composition, cation distribution, valence states of Fe and Mn ions, and magnetic properties. The discharge capacity depends not only on the 3d metal ion ordering up to 650 °C but also on their primary particle size and lithium content responsible for the iron valence state.

Results described herein can explain why previous attempts[5,6] failed to use the Fe^{3+} ion in $LiFe_xM_{1-x}O_2$ (M = Co and Ni) as an electrochemically active component because their preparation conditions were not optimized for maximizing discharge capacity from Fe^{3+}/Fe^{4+} redox because of high-temperature heat treatment above 700 °C.

These results reveal the importance of the synthetic route for iron oxide based positive electrode materials. To reduce firing temperature and primary particle size, homogeneous mixing of Fe and other 3d cations is necessary because Fe^{3+}/Fe^{4+} redox was observed only in the solid solution of $LiFeO_2$ with $LiCoO_2$,[7,21] $LiNiO_2$,[8,19] Li_2MnO_3,[9,10] or Li_2TiO_3.[4] The maximum discharge capacity was obtained around unity for the Fe/other 3d cation ratio. The development of liquid-phase synthesis including coprecipitation and hydrothermal reaction methods might reveal a novel iron oxide based positive electrode material through combination with a novel material design concept.

Acknowledgment. We express our gratitude for financial support from The New Energy and Industrial Technology Development Organization (NEDO) and the Ministry of Economy, Trade and Industry (METI), and for valuable advice from Dr. Tatsuya Nakamura of the University of Hyogo.

CM050095+